Supporting Information

Particles' nanosizing and coating by an ionic liquid: two routes to improve transport properties of $Na_3V_2(PO_4)_2FO_2$

Jacob Olchowka [a,d,e,*], Runhe Fang [b,d], Rafael Bianchini Nuernberg [a], Chloé Pablos [a,c,d], Dany Carlier [a,d,e], Sophie Cassaignon [b,d,*], Laurence Croguennec [a,d,e]

[a] Univ. Bordeaux, CNRS, Bordeaux INP, ICMCB, UMR 5026, F-33600 Pessac, France

[b] Sorbonne Université, CNRS, Laboratoire Chimie de la Matière Condensée de Paris, LCMCP, UMR 7574, 4 Place Jussieu, 75005 Paris, France

[c] Laboratoire de Réactivité et de Chimie des Solides, Université de Picardie Jules Verne, CNRS-UMR 7314, F-80039 Amiens Cedex 1, France

[d] RS2E, Réseau Français sur le Stockage Electrochimique de l'Energie, CNRS 3459, 80039 Amiens Cedex 1, France

[e] ALISTORE-ERI European Research Institute, CNRS 3104, 80039 Amiens Cedex 1, France

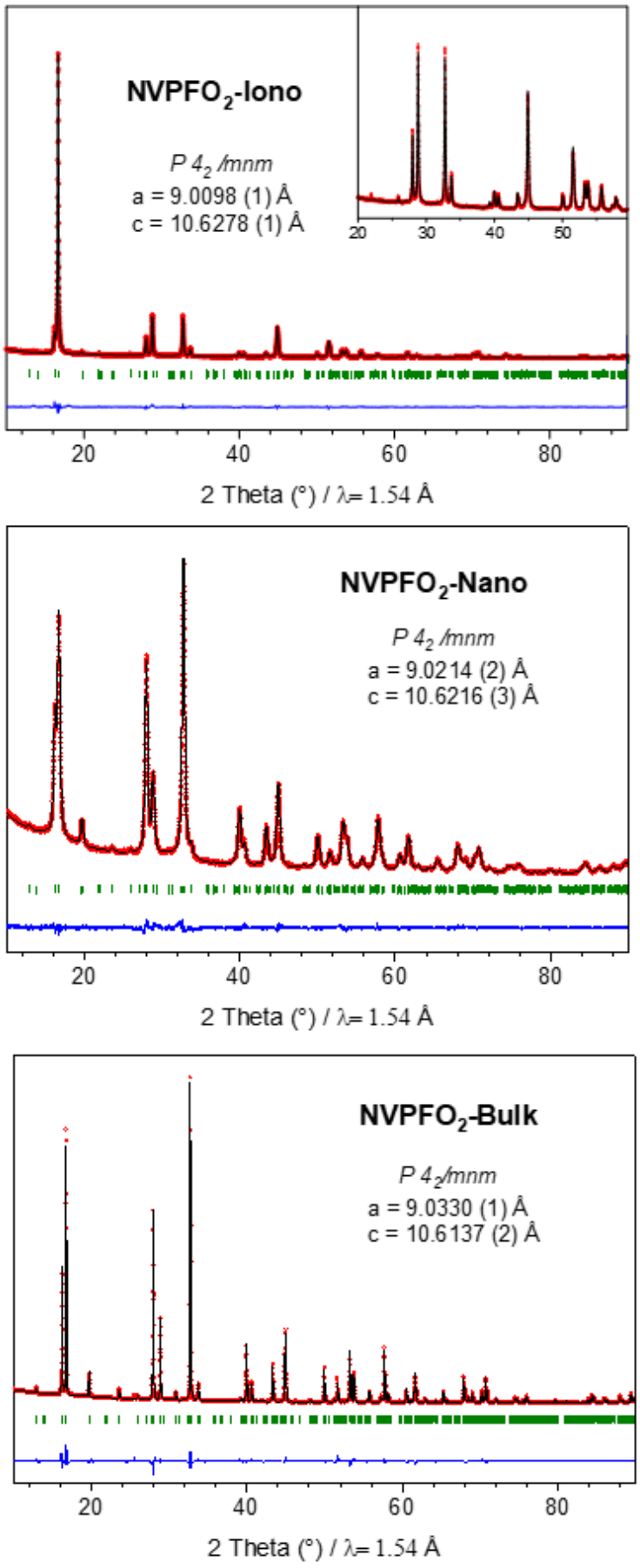

Figure S1. Rietveld refinement of $NVPFO_2$-Iono, $NVPFO_2$-Nano and $NVPFO_2$-Bulk.

In this work, $NVPFO_2$ materials are refined in the "average" space group *$P4_2/mnm$*, due to the limited resolution of the laboratory equipment. Indeed, with Synchrotron data, Nguyen et al. found that an ordering of Na^+ happens along the crystallographic *b* and *c* axes and the accurate $NVPFO_2$ structure should be described in the monoclinic *$P2_1/m$* space group with a modulation vector q = ½ b* + ½ c*.[1]

Table S1. Cationic ratio determined by ICP-OES

Sample	$NVPFO_2$-Iono	$NVPFO_2$-Nano	$NVPFO_2$-Bulk
Na/V/P	2.9(1) : 2.0 (1) : 2.0 (1)	3.0(1) : 2.0 (1) :2.0 (1)	2.9(1) : 2.0 (1) : 2.0 (1)

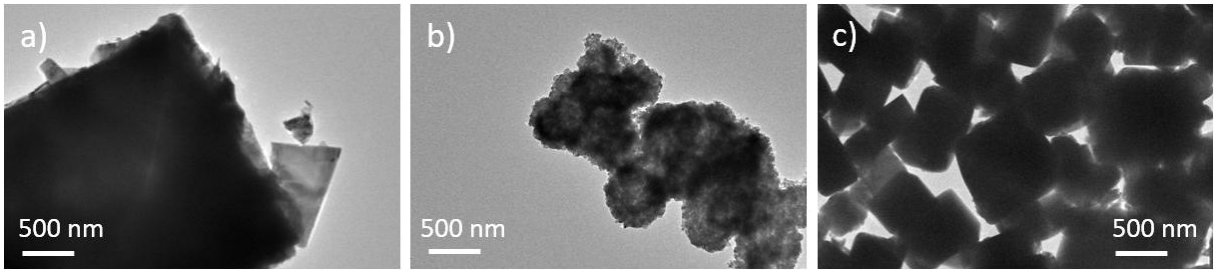

Figure S2. TEM images of a): $NVPFO_2$-Iono, b): $NVPFO_2$-Nano, c): $NVPFO_2$-Bulk.

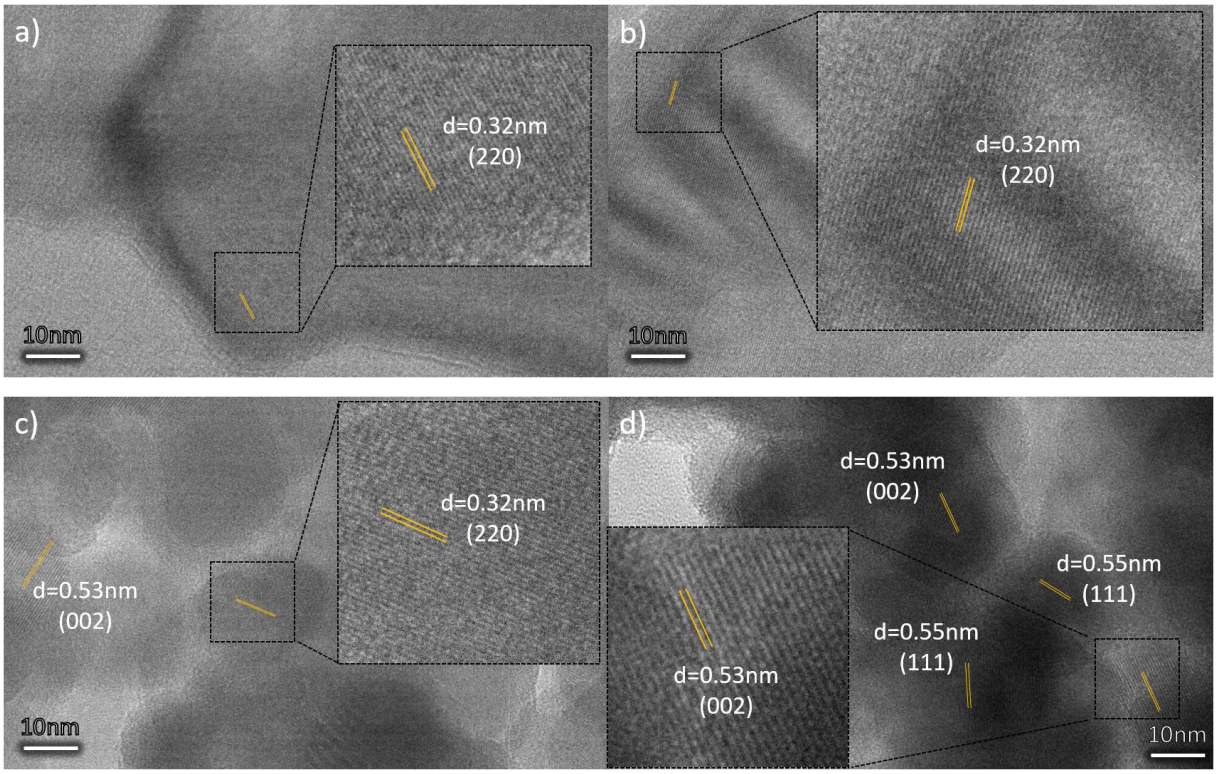

Figure S3. a), b): HRTEM for $NVPFO_2$-Iono; c), d): HRTEM for $NVPFO_2$-Nano.

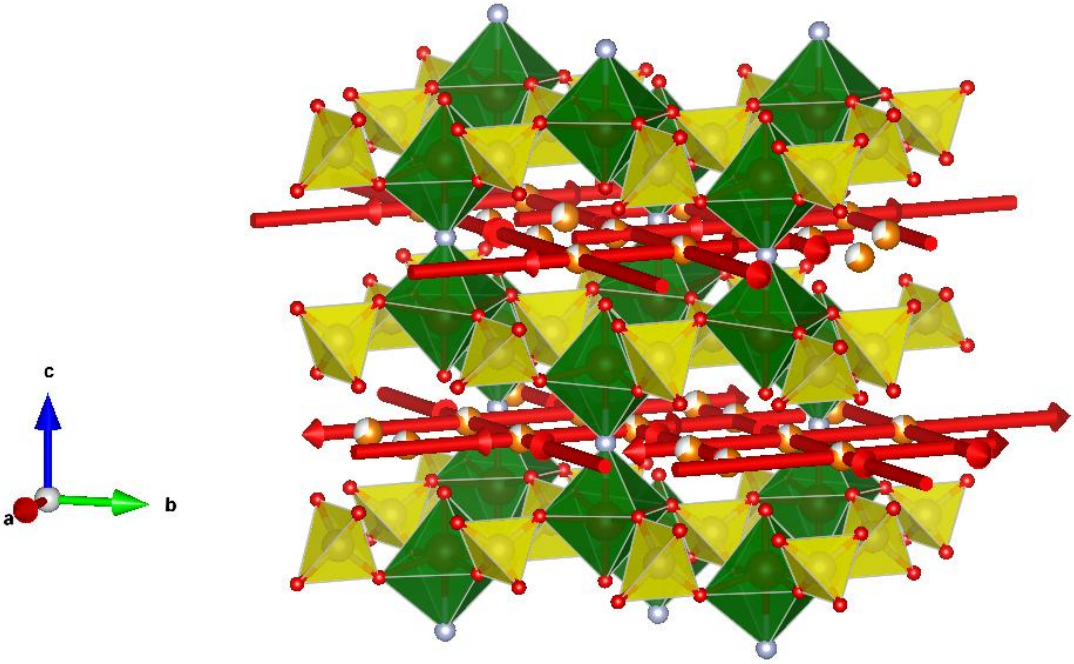

Figure S4. Illustration of $Na_3V_2(PO_4)FO_2$ crystal structure, the vanadium octahedra are depicted in green, the phosphate in yellow and sodium ion in orange/grey. The sodium diffusion channels are represented by red arrow and correspond to [110] and [1-10] directions in the (ab) plane.

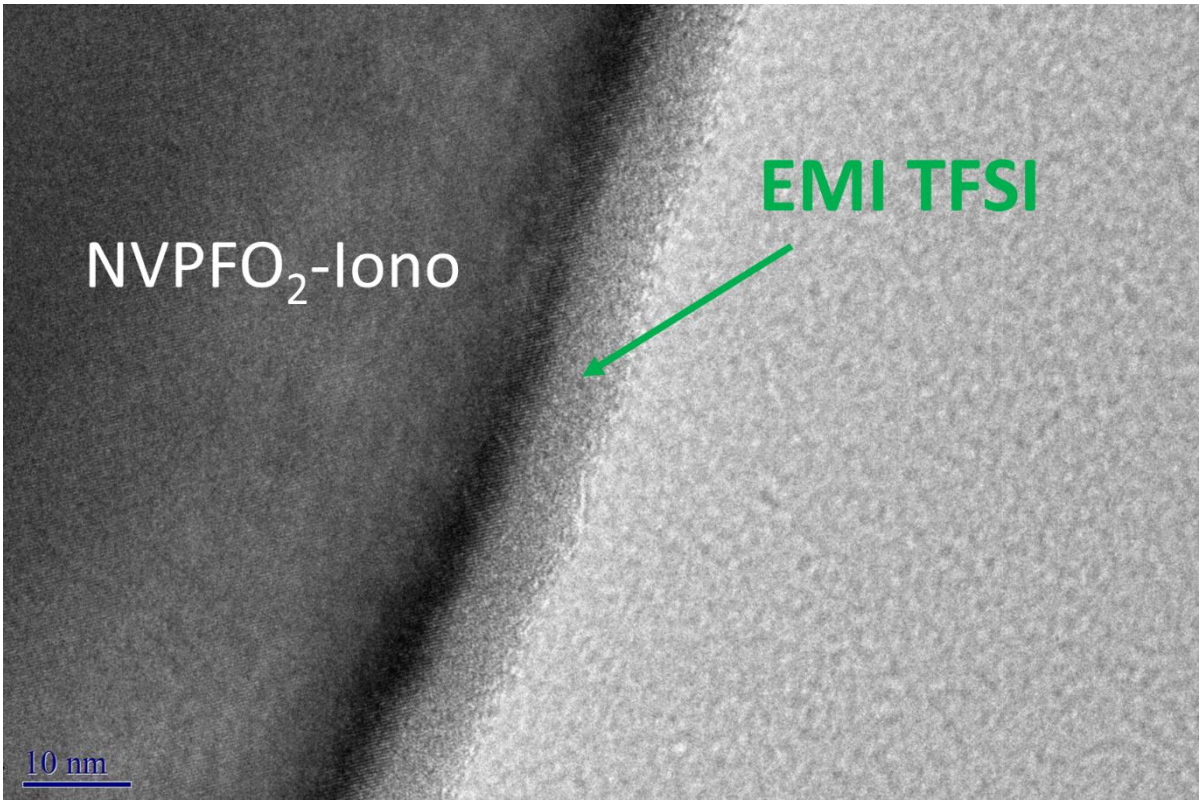

Figure S5. HRTEM for $NVPFO_2$-Iono, the presence of an amorphous coating on the surface of the platelets confirms the presence of the EMI TFSI ionic liquid.

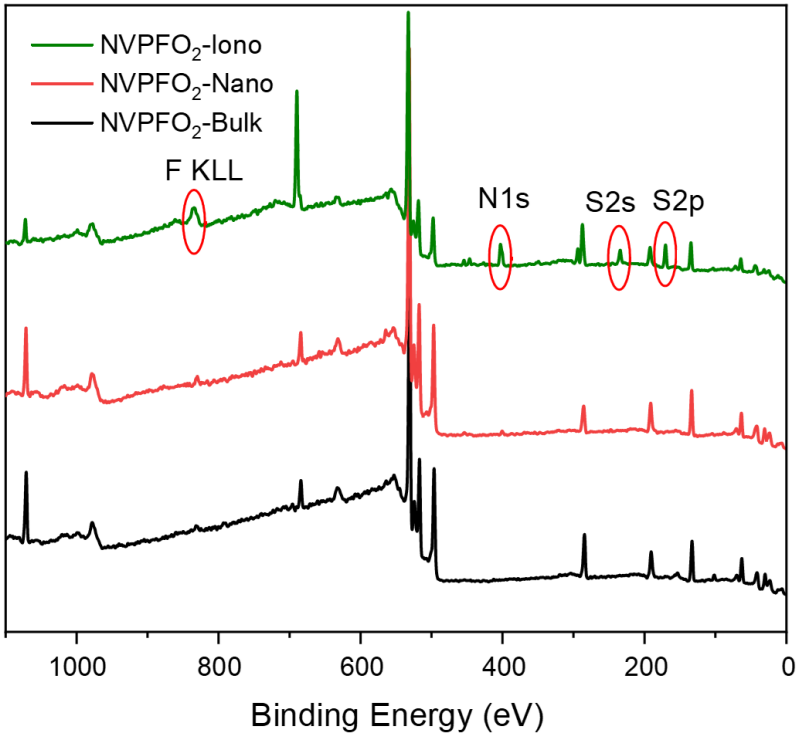

Figure S6. XPS spectra of all the $NVPFO_2$ materials.

Table S2. Quantification of V, P and F from XPS spectra

Sample	$NVPFO_2$-Iono	$NVPFO_2$-Nano	$NVPFO_2$-Bulk
V at.%	1.48	2.44	2.60
P at.%	5.60	8.49	8.47
F at.%	8.74	1.70	1.92

The higher amount of fluorine vs vanadium and phosphorus for $NVPFO_2$-iono clearly demonstrated that the ionic liquid covers the surface of $Na_3V_2(PO_4)_2FO_2$.

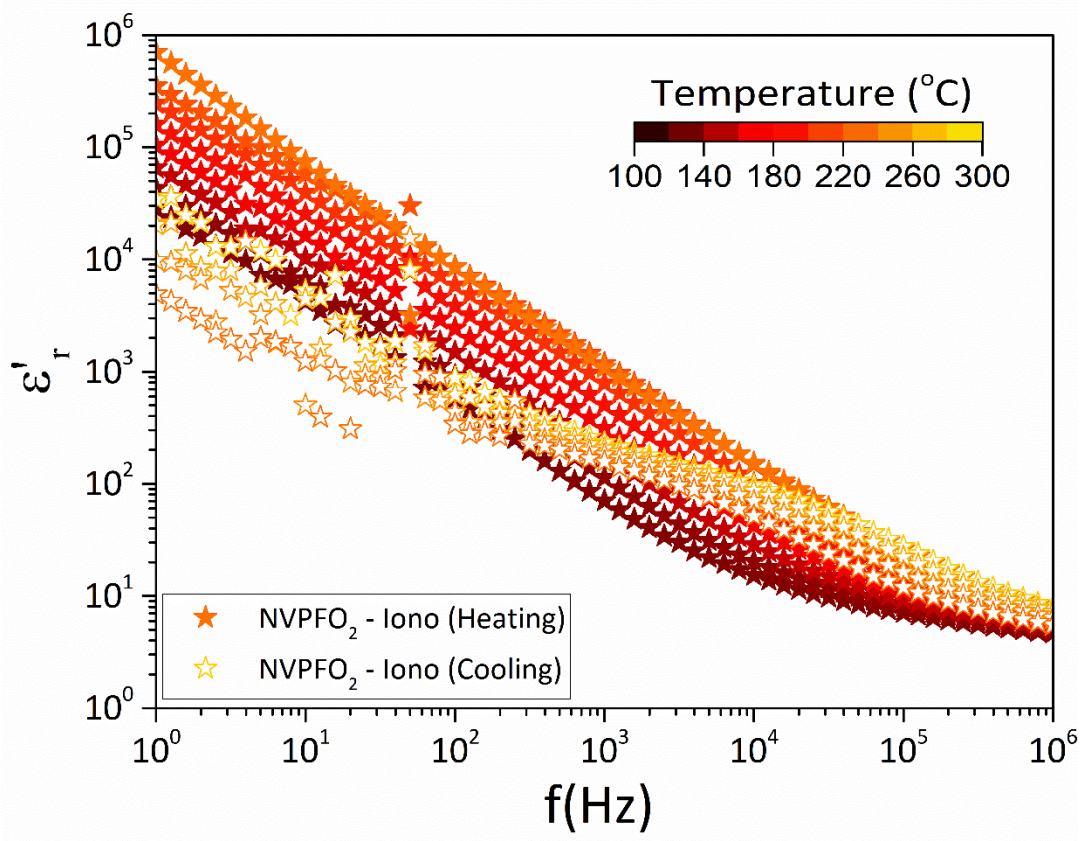

Figure S7 - Dependence of the real part of the relative permittivity on frequency at different temperatures for samples $NVPFO_2$-Iono under heating and cooling. The presented results have been normalized by the shape factor of the specimen and vacuum permittivity.

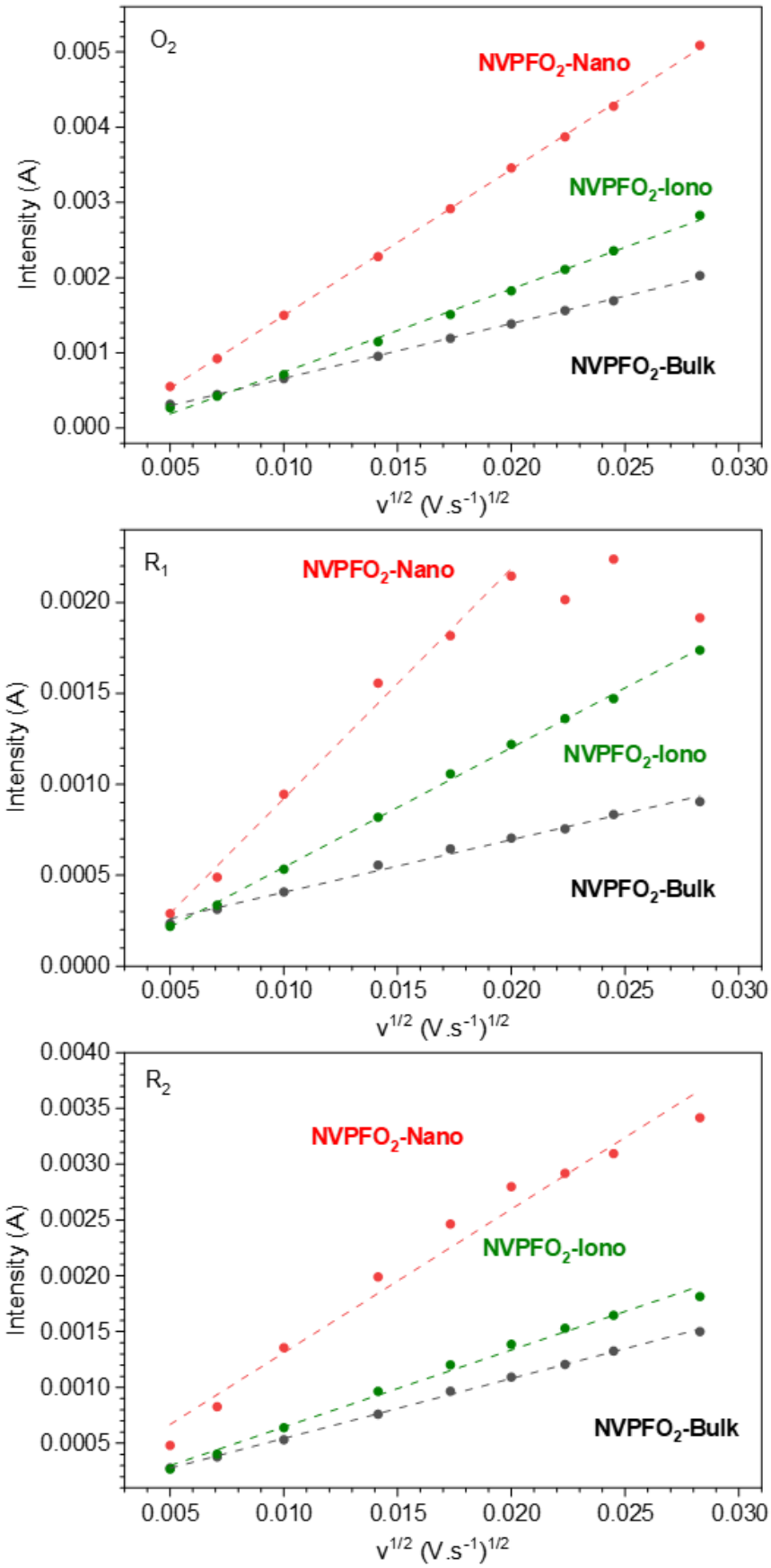

Figure S8. Linear fitting curves between the redox peak current and the square root of the scan rate of O_2 peak, R_1 peak and R_2 peak.

All the ionic diffusion coefficients were determined from the Randles-Sevcik equation (**eq.1**).

$$i_p = 0.4463nFAC\frac{nFvD}{RT}^{\frac{1}{2}} \quad (1)$$

Where i_p is the maximum current in A, n is the number of electrons transferred in the redox event (n=1), A is the electrode area (2 cm²), F is the Faraday constant, C is the concentration of Na^+ (12 Na^+ in a unit cell of 866.75 $Å^3$ lead to 0.02 mol/cm^3), *v* is the scan rate ($V.s^{-1}$), R is the gas constant and T is the temperature in Kelvin.

Here we approximate the electrode surface area to 2 cm² (without taking into account the specific surface area (SSA) of the electrode material nor the electrode porosity). This allows to give a reliable comparison between the three electrode materials. Indeed, according to some recent work, we do not think that SSA of active materials is the electrochemical active area, since the uptake of charge carriers in electrodes is anisotropic, namely not all the surfaces are active for the insertion of charge carriers.[2] As the geometric surface area considered in this work is different from the electrochemical active surface area, calculated coefficient diffusion are overestimated compared to their actual values. Nevertheless, we could measure SSA of NVPFO2-Nano and NVPFO2-Bulk which are 10.8 m²/g and 2 m²/g respectively

Part S9-S10. GITT measurements and diffusion coefficients calculation.

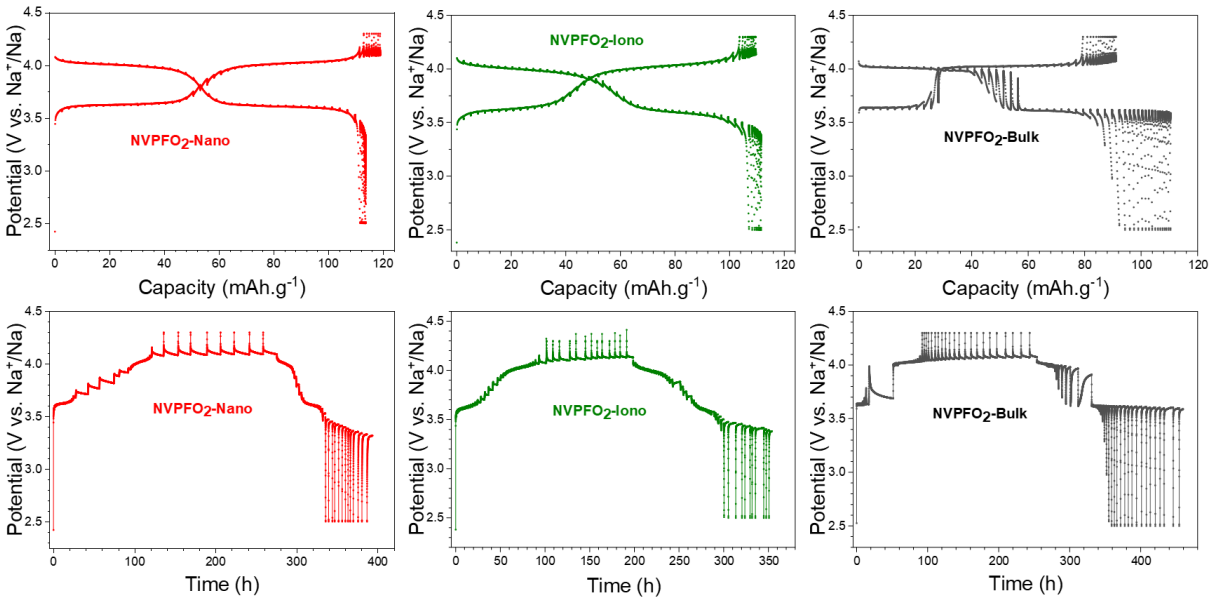

Figure S9. GITT results of the $NVPFO_2$ materials with Potential versus capacity and potential versus time.

On the basis of the GITT measurement, the chemical diffusion coefficients of sodium ions for the three materials were calculated by the following simplified formula (**eq.2**) with rather small pulse current and short time intervals. However, it should be noticed that the determination of diffusion coefficient presented below is just a first approximation as part of the reaction mechanism is of first order (biphasic domains)[3] which not allow using this formula due to consequent structural modification during the desodiation process.

$$D = \frac{4}{\pi\tau}\left(\frac{m_B V_M}{M_B S}\right)^2 \left(\frac{\Delta E_S}{\Delta E_\tau}\right)^2 \quad (2)$$

The slow changes of potential are associated to the diffusion of Na^+ while the sharp potential rise or drop can be attributed to charge transfer and ohm resistance.[4] GITT curves show for all the $NVPFO_2$ materials an increasingly larger overpotential towards the end of charge/discharge, implying a kinetically limited process. However, it is much more pronounced for $NVPFO_2$-Bulk than for the two others electrode materials. This overpotential can also be clearly identified during the potential jump between the first and the second plateaus for $NVPFO_2$-Bulk (**Figure S9 and S10c**). In practice this generates heat and can lead to the degradation of long-term stability. On the other hand, for $NVPFO_2$-Nano and $NVPFO_2$-Iono, this variation is not obvious. More detailed comparisons can be seen from the **Figure S10d** with the calculated overpotential for each material represented in the inset.

Figure S10 depicts also the variation of the average diffusion coefficient along the charging/discharging processes. Generally, all the compounds suffer a decrease in diffusion coefficient before the 50% state of charge/discharge followed by a small lift because of the easier sodium ion extraction process. Then, it continuously decreases until the state of full/none sodium ion. A bigger diffusion coefficient for the sodium deintercalation process (oxidation) is observed for all the materials with the best 1.11×10^{-10} cm^2s^{-1} for $NVPFO_2$-Nano. Their mean diffusion coefficients during Na^+ insertion and extraction are listed below (**Table S2**). All the results correspond well to the tendency of those obtained by CV analysis. The sodium ion diffusion advantages of nanospherical morphology is thus verified once again.

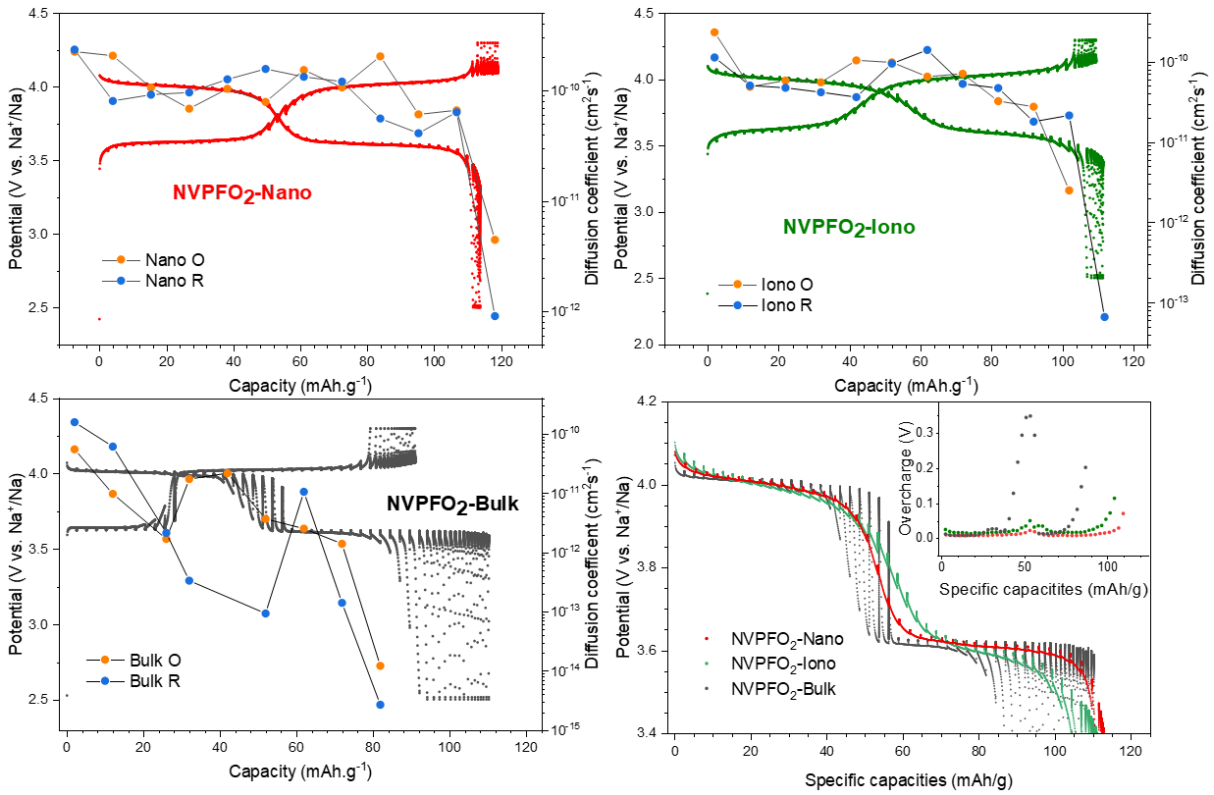

Figure S10. a), b) and c): GITT test results of the $NVPFO_2$ electrode obtained by different synthesis methods, showing the changes of $D_{app,Na}$ and potentials along with the GCD processes. d): GITT electrochemical discharge curves of all the $NVPFO_2$ materials. Inset: overpotential between discharge and relaxation intervals.

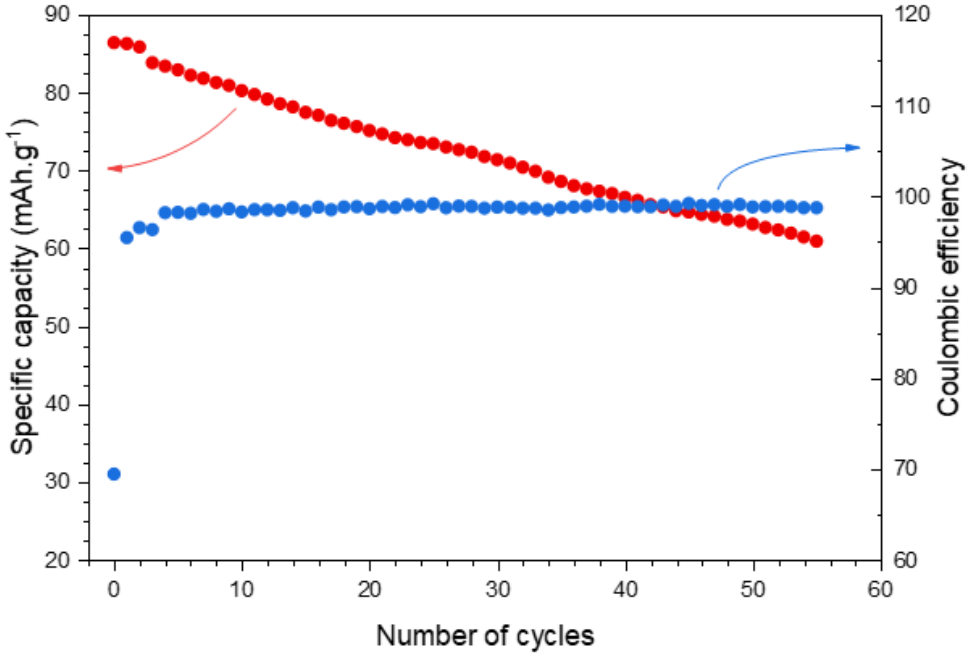

Figure S11. Evolution of reversible capacity upon long term cycling and the coulombic efficiency of the $NVPFO_2$-Nano vs. HC (hard carbon) full cell.

Bibliography:

(1) Nguyen, L. H. B.; Broux, T.; Camacho, P. S.; Denux, D.; Bourgeois, L.; Belin, S.;

Iadecola, A.; Fauth, F.; Carlier, D.; Olchowka, J.; et al. Stability in Water and Electrochemical Properties of the Na3V2(PO4)2F3 – Na3(VO)2(PO4)2F Solid Solution. *Energy Storage Mater.* **2019**, *20* (April), 324–334. https://doi.org/10.1016/j.ensm.2019.04.010.

(2) Yang, X.; Rogach, A. L. Electrochemical Techniques in Battery Research: A Tutorial for Nonelectrochemists. *Adv. Energy Mater.* **2019**, *9* (25), 1–10. https://doi.org/10.1002/aenm.201900747.

(3) Sharma, N.; Serras, P.; Palomares, V.; Brand, H. E. A.; Alonso, J.; Kubiak, P.; Fdez-Gubieda, M. L.; Rojo, T. Sodium Distribution and Reaction Mechanisms of a Na 3 V 2 O 2 (PO 4) 2 F Electrode during Use in a Sodium-Ion Battery. *Chem. Mater.* **2014**, *26* (11), 3391–3402. https://doi.org/10.1021/cm5005104.

(4) Cai, Y.; Cao, X.; Luo, Z.; Fang, G.; Liu, F.; Zhou, J.; Pan, A.; Liang, S. Caging Na3V2(PO4)2F3 Microcubes in Cross-Linked Graphene Enabling Ultrafast Sodium Storage and Long-Term Cycling. *Adv. Sci.* **2018**, *2*, 1800680. https://doi.org/10.1002/advs.201800680.